ELSEVIER

Journal of Power Sources 81–82 (1999) 585–588

JOURNAL OF POWER SOURCES

www.elsevier.com/locate/jpowsour

Advanced lithium ion cells with lithium manganese spinel

Peter Bäuerlein *, Rudolf Herr, Matthias Kloss, Jörg Kümpers, Matthias Maul, Eberhard Meissner

Varta AG Research and Development Center, Gundelhardtstraße 72, D-65779 Kelkheim, Germany

Abstract

For electric vehicle propulsion, a number of alternative concepts exist. One approach is the so-called full electric vehicle (EV), which is exclusively driven by a battery. Another alternative is the hybrid vehicle concept, where a combustion engine and a battery are used for propulsion. Both concepts differ in the requirements for the battery used. This leads to the fact that for each application a special type of battery has to be tailored, resulting in a high-energy battery for the EV application and a high-power battery for hybrid vehicles. Both requirements, the high-energy and the high-power requirement, can be met by lithium ion batteries. With lithium manganese oxide and carbon as active materials, high-energy cells were realised with an energy density of 115 Wh/kg and a specific pulse power of 500 W/kg, as well as high-power cells with an energy density of 60 Wh/kg and a specific pulse power of 850 W/kg. Both types of cells show good cycle life and good performance at low temperatures.

Keywords: Lithium ion batteries; Lithium manganese spinel; Energy density; High-power performance; Low temperature performance; Cycle life

1. Introduction

A high gravimetric and volumetric energy density is the key feature of the lithium ion system [1,2]. Therefore, it is expected to be the dominating technology for electric vehicles (EV) and aerospace applications. Hybrid vehicles, however, will be driven by an internal combustion engine and a small high-power battery, which buffers the energy spikes during acceleration and braking. The high-power and the high-energy requirements can be met by lithium ion batteries. With lithium manganese oxide [3–5] as a cathode material and carbon [6,7] as an anode material, a high-energy density and a good power capability can be achieved.

The lithium ion system can work within a wide temperature range of −20 to 60°C. Therefore, it fits well for the applications mentioned above. Nevertheless, lifetime, high rate performance and low temperature performance are still challenging requirements for lithium ion batteries.

2. Experimental

High-energy cells are manufactured from a dry rolled cathode, where the mass mixture, consisting of active material, binder and conductive filler, is pressed into aluminium-expanded metal via a rolling process. A wet pasted carbon electrode is used as anode. This electrode is made by pasting a slurry, consisting of carbon, binder, conductive filler and a solvent, into nickel foam. The electrodes are dried prior to use and stacked into a prismatic cell case.

The high-power cell consists of jet coated electrodes. *N*-methylpyrrolidone (NMP) is used as a solvent to produce a slurry, which is coated onto the current collector substrates, an aluminium foil in case of the cathode and a copper foil in case of the anode. The electrodes are dried, then a jelly roll is fabricated and transformed into a cylindrical cell case. A lithium salt ($LiPF_6$) dissolved in a mixture of carbonate solvents (EC, DEC, DMC etc.) is used as electrolyte [8,9]; microporous polyolefin is used as a separator.

3. Results and discussion

3.1. Pulse power and continuous discharge power performance

The Ragone diagram for continuous discharge currents is shown in Fig. 1. The discharges are performed at ambient temperatures, starting with a C/5 rate, ending up with a 10 C rate for the high-power design and a 5 C rate for the high-energy design.

* Corresponding author. Tel.: +49-6195-802-322; Fax: +49-6195-802-337; E-mail: peter.baeuerlein@varta.com

0378-7753/99/$ - see front matter
PII: S0378-7753(99)00226-8

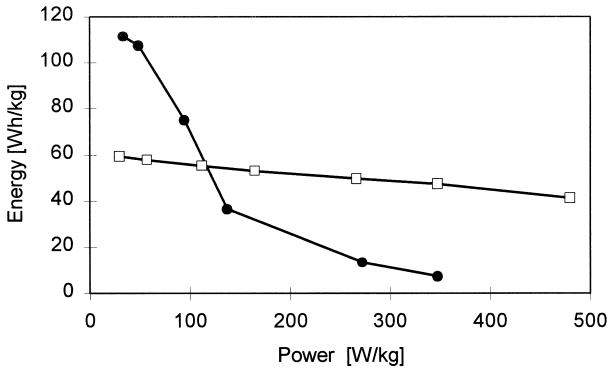

Fig. 1. Ragone diagram; (□) high-power design; (●) high-energy design.

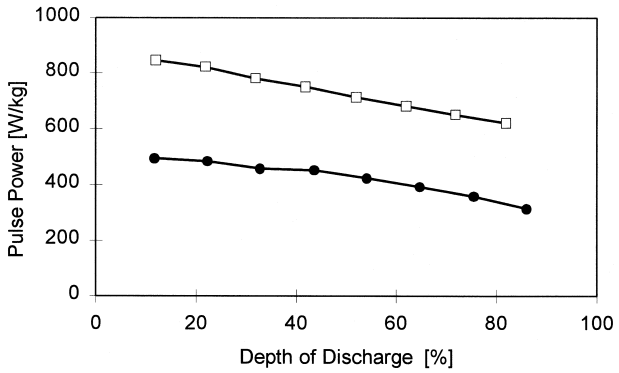

Fig. 3. Pulse power performance; (□) high-power design (10 C pulses); (●) high-energy design (1 C pulses).

The energy density of 115 Wh/kg of the high-energy design is obtained at a discharge power of 30 W/kg. For high-power discharges at more than 100 W/kg, the energy density decreases quite rapid. The energy density of the high-power design for the hybrid vehicle application, however, declines only little over a wide range of discharge power. For a continuous discharge power of 480 W/kg, which is equal to a 10 C rate, a energy density of more than 40 Wh/kg can be obtained. This is about 70% of the energy density, which can be obtained at a discharge power of 30 W/kg.

The pulse power at a certain DOD (PP_{DOD}) is calculated from Eq. (1), where 3.0 V is defined to be the cut off voltage. OCV_{DOD} is the open circuit voltage at a certain DOD and R_{DOD} is calculated from a discharge pulse at a certain DOD as shown in Fig. 2.

$$PP_{DOD} = 3.0\ V\,(OCV_{DOD} - 3.0\ V)/R_{DOD} \quad (1)$$

Both cell designs show a good pulse power performance over a wide range of DOD (see Fig. 3). The discharge pulses are performed at ambient temperatures. For the high-energy design, a pulse current corresponding to a 1 C rate was performed, whereas for the high-power design a pulse current corresponding to a 10 C rate was applied. The high-energy cell results in a specific pulse power of 500 W/kg at 10% DOD, declining to 320 W/kg at 80% DOD. The high-power cell however, is on a higher pulse power level of about 850 W/kg at 10% DOD, decreasing to 620 W/kg at 80% DOD.

3.2. Influence of temperature

Fig. 4 shows the discharge curves for a high-energy cell at different rates. More than 40% of the C/5 capacity of a high-energy cell can be obtained at discharge rate of 1.7 C at 20°C, whereas only 10% are obtained at −20°C at the same rate. A discharge at 3.3 C rate at 20°C reduces the cell capacity to 16% of the C/5 capacity, at −20°C only 7% can be obtained at this rate. The discharge voltage also decreases significantly with increasing discharge power and decreasing temperature, as shown in Table 1. For a discharge with 3.3 C rate at 20°C, an average discharge voltage of 3.23 V is observed, declining to 2.52 V at −20°C.

Fig. 5 shows the discharge curves for a high-power cell at different rates. Compared to the high-energy cell, the high-power cell shows significantly higher discharges voltages at a certain rate, especially at low temperature. A discharge with 5 C rate results in an average discharge

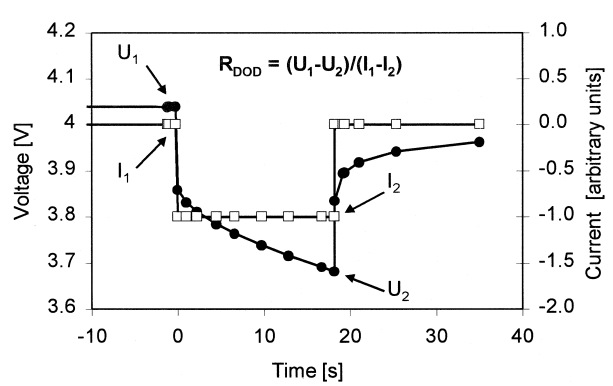

Fig. 2. Discharge pulses at a certain DOD; (□) current; (●) voltage.

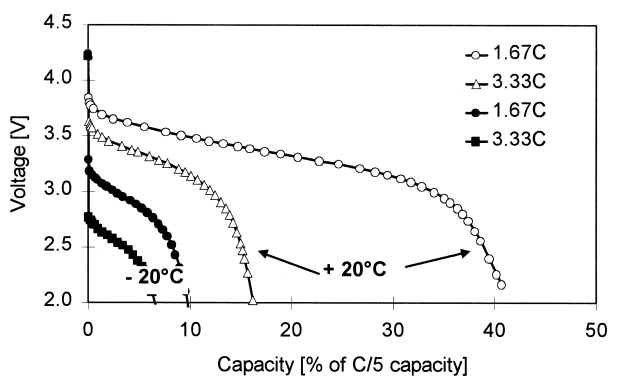

Fig. 4. High-energy cell; discharge curves at different rates and different temperatures.

Table 1
Average discharge voltage and energy density of high-energy and high-power cell designs as a function of temperature and discharge power

	Power (W/kg)	Energy (Wh/kg)	Voltage (V)
High-power cell +20°C	68	52.0	3.79
	135	48.7	3.68
	216	46.8	3.60
	374	41.9	3.42
High-power cell −20°C	54	36.6	3.00
	107	35.0	2.92
	167	31.9	2.78
	284	28.0	2.60
High-energy cell +20°C	151	37.0	3.32
	294	14.3	3.23
	375	7.0	2.75
High-energy cell −20°C	131	7.7	2.88
	229	4.5	2.52
	273	0.2	2.00

voltage of 3.60 V, which decreases to 2.78 V at −20°C. About 85% of the C/5 capacity of a high-power cell can be obtained at a discharge rate of 9 C at 20°C, at −20°C still more than 70% of this capacity can be obtained at the same rate. The voltage curve at −20°C, however, shows a remarkable shape at high discharge rates. Even at 5 C rate, a small increase in the discharge voltage is observed with discharge time. This effect is more obvious at 9 C rate, where the discharge voltage drops below 2.3 V in the beginning when about 10% of the nominal capacity are reached. After about one minute, an increase to more than 2.6 V at approximately 50% of the nominal capacity are observed. This effect is related to the self heating of the high-power cell during a high rate (> 5 C) discharge.

From the data in Table 1, a Ragone diagram was calculated (Fig. 6), representing the high rate regions for the different types of cell designs at +20°C as well as −20°C. As one could expect, the rate capability decreases with decreasing temperature. The curve for the high-power cell is shifted in parallel to lower energy densities with

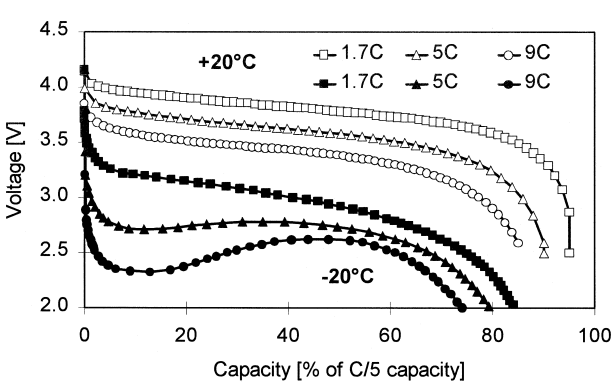

Fig. 5. High-power cell; discharge curves at different rates and different temperatures.

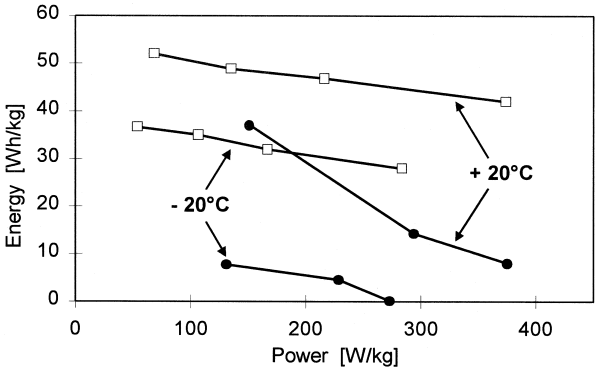

Fig. 6. Ragone diagram for at +20°C and −20°C; (□) high-power design; (●) high-energy design.

decreasing temperature. A discharge with 9 C rate which is equal to 374 W/kg at +20°C or 284 W/kg at −20°C, leads to an energy density of 42 Wh/kg at +20°C and 28 Wh/kg at −20°C. A discharge of the high-energy cell at the 5 C rate, which is equal to 375 W/kg at 20°C or 273 W/kg at −20°C, results in an energy density of 7 Wh/kg at +20°C and 0.2 Wh/kg at −20°C. The significant difference in the high rate and low temperature behaviour can be related to the voltage curves, which have been shown already in Figs. 4 and 5. The discharge voltage at high rates and low temperatures is significantly lower for the high-energy cell, due to higher ohmic resistance and higher polarisation.

3.3. Cycle life

Due to the different rate capability, 100% DOD discharges are performed at different rates for the two types of cells. A discharge at 1 C rate is used for the high-power cell, whereas the high-energy cell is discharged at a C/5 rate. Both types of cells show a good cycle life as shown in Fig. 7. Even after 600 cycles the cell capacity exceeds 80% of the nominal capacity for both types of cells. Also, the capacity fading per cycle is comparable for both types

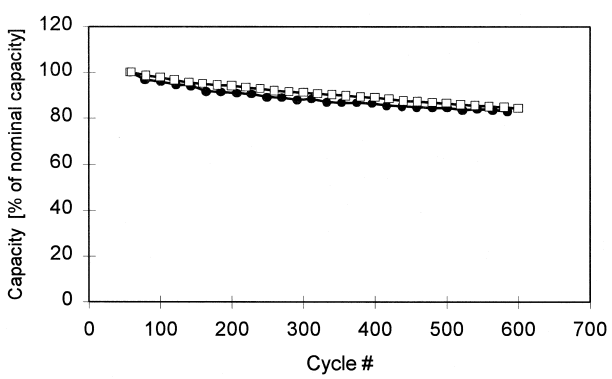

Fig. 7. Cycle life of high-energy and high-power lithium ion cells; (□) high-power cell—1 C @ 100% DOD; (●) high-energy cell—C/5 @ 100% DOD.

Table 2
Summarised results of the different cell designs

	High-energy cell	High-power cell
Energy density @ C/5 (Wh/kg)	115	60
Energy density @ C/5 (Wh/l)	270	170
Pulse power @ 10% DOD (W/kg)	500	850
Pulse power @ 80% DOD (W/kg)	320	620
Energy density @ 5C, 20°C (Wh/kg)	7	47
Energy density @ 5C, −20°C (Wh/kg)	0.2	32
Capacity fading (% per cycle)	0.03	0.03

of cells; the capacity loss is calculated to 0.03% per cycle. From these values, a cycle life (> 80% of nominal capacity) of more than 800 full cycles (100% DOD) can be estimated.

4. Summary and conclusions

At low rates, the high-energy design shows a significantly higher energy density of 115 Wh/kg (270 Wh/l), compared to the high-power cell design, which has an energy density of 60 Wh/kg (170 Wh/l). At high rates and at lower temperatures, the high-power cell design provides a higher energy density and discharge voltage curve. Both types of cells show a good pulse power performance—the high-power cell, however, on a significantly higher pulse power level. Both types of cells also show good cycle life. More than 600 cycles are performed so far, the cell capacity still exceeds 80% of their nominal capacity. The results are summarised in Table 2.

For the different concepts of electric propulsion, different battery cell designs are needed. The battery has to be tailored to the high-power or the high-energy application. Lithium ion batteries with lithium manganese oxide cathodes can meet the demands of both applications. Therefore, this battery system is one of the most promising for electric vehicles and for hybrid vehicles.

Acknowledgements

Support for research and development of large Lithium Ion cells and batteries at VARTA by the DOE of the United States under USABC and PNGV contracts, by the German Federal Ministry for Education and Research (BMBF), and by the Commission of the European Union is highly appreciated. The authors thank their numerous colleagues not named individually for their valuable contributions.

References

[1] K. Brandt, J. Power Sources 54 (1995) 151.
[2] S. Megahed, B. Scrosati, J. Power Sources 51 (1994) 79.
[3] M.M. Thackeray, A. de Kock, M.H. Rossouw, D. Liles, R. Bitthin, D. Hoge, J. Electrochem. Soc. 139 (1992) 363.
[4] T. Ohzuku, M. Kitagawa, T. Hirai, J. Electrochem. Soc. 137 (1990) 769.
[5] D. Guyomard, J.M. Tarascon, Solid State Ionics 69 (1994) 222.
[6] R. Fang, M. von Sacken, J.R. Dahn, J. Electrochem. Soc. 137 (1990) 2009.
[7] T. Ohzuku, Y. Iwakoshi, K. Sawai, J. Electrochem. Soc. 140 (1993) 2490.
[8] S. Tobishima, K. Hayashi, K. Saito, J. Yamaki, Electrochim. Acta 40 (1995) 537.
[9] D. Aurbach, Y. Ein-Eli, B. Markovsky, A. Zuban, J. Electrochem. Soc. 142 (1995) 2882.